Hysteresis in modeling of poroelastic systems: Quasistatic equilibrium

R. A. Guyer[*]
Los Alamos National Laboratory, Los Alamos, New Mexico, 87545, USA, and Department of Physics, University of Nevada, Reno, Nevada 89577, USA

H. Alicia Kim[†]
Department of Mechanical Engineering, University of Bath, Bath BA2 7AY, United Kingdom

Dominique Derome[‡]
Wood Laboratory, Swiss Federal Laboratory for Materials Science and Technology, EMPA, Uberlandstrasse 129, CH-8600 Dubendorf, Switzerland

Jan Carmeliet[§]
ETH Zurich, HIL E46.3, Wolfgang-Pauli-strasse 15, CH-8093 Zurich, Switzerland and Laboratory for Building Science and Technology, Swiss Federal Laboratory for Materials Science and Technology, EMPA, Uberlandstrasse 129, CH-8600 Dubendorf, Switzerland

J. TenCate[‖]
Geophysics, Earth and Environmental Sciences MS D443 Los Alamos National Laboratory Los Alamos, New Mexico 87545, USA

(Received 16 November 2010; revised manuscript received 25 April 2011; published 28 June 2011)

The behavior of hysteretic, coupled elastic and fluid systems is modeled. The emphasis is on quasistatic equilibrium in response to prescribed chemical potential (μ) protocols and prescribed stress (σ) protocols. Hysteresis arises in these models either from the presence of hysterons or from the presence of self-trapping internal fields. This latter mechanism is modeled in finite element calculations which serve to illustrate the creation of hysteresis in a range of circumstances that go from conventionally hysteretic systems, a sandstone, to systems like a wood fiber. An essential ingredient in the behavior of these systems, the interaction between the mechanical variables and the fluid variables, is accorded special attention. The proper venue for the exploration of these systems is (μ,σ) space and appropriate μ protocols, σ protocols, and combined μ-σ protocols.

DOI: 10.1103/PhysRevE.83.061408 PACS number(s): 82.33.Ln, 68.43.−h, 46.15.−x

I. INTRODUCTION

In order to have a sample large enough for easy measurement a low-temperature experimentalist forms a two-dimensional Fermi fluid on a Nuclepore filter [1]. Quantification of the properties of the Fermi fluid depend on knowledge of the surface area on which it resides. The area is found from measurement of an adsorption isotherm [2]. Resonant bar measurements on a Berea sandstone show nonlinear behavior at modest strain levels that can be related to hysteretic features found on subjecting the sandstone to elaborate stress-strain testing [3]. The principles that inform the preparation of wood products for use are learned in laboratory studies of *shrinkage while drying* or *moisture induced stress*, that is, studies of the stress-strain consequences of exposing a wood sample to moisture [4]. In these examples the response, a strain or a change in moisture content, is a hysteretic function of the field that drives the system, a stress or a chemical potential. A typical material having this type of response is a porous material, for example, a Nuclepore filter [2], a sandstone [3], or a wood fiber [4].

In this paper we describe two schemes for modeling materials with hysteretic response. Macroscopic hysteresis is present either as a deliberate input (mesoscopic hysteretic elements, hysterons [5]) or as a consequence of *self-trapping* internal fields. The latter source of hysteresis, analogous to that in a random field Ising model [6], is new in the present context. These two sources of hysteresis touch two different physical limits represented by (1) capillary condensation involving instabilities that connect mesoscopic fluid configurations and by (2) moisture uptake by a fiber that couples strongly to the mechanical state of the fiber.

In this modeling the mesoscopic features in the model are endowed with hysteretic properties. In physical realizations of the modeled systems the hysteresis is conferred by microscopic entities whose precise internal working are complex and possibly not well understood. The purpose of the phenomenology is to establish the structure of an appropriate model, for example, symmetries with respect to the fields involved, couplings among the fields, and in the present context the etiology of hysteretic behavior. As an example of the latter suppose there is hysteretic fluid content in response to a chemical potential drive and attending hysteretic strain. Does this imply a hysteretic fluid response to an applied stress? Within the domain of Landau theory [7] this question has a definite answer. As we may be outside of that domain and the domain of reversible thermodynamics the answer to such a question is very much a part of model construction.

[*]guyer@physics.umass.edu
[†]h.a.kim@bath.ac.uk
[‡]Dominique.Derome@empa.ch
[§]Jan.Carmeliet@empa.ch
[‖]tencate@lanl.gov

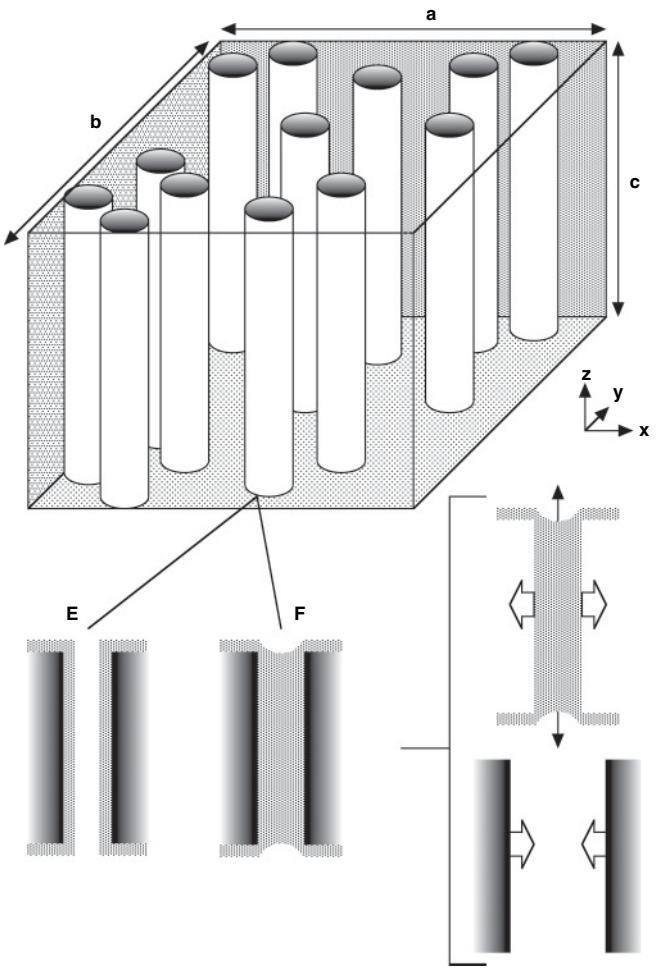

FIG. 1. System. A set of parallel pores of length c, areal density n_A (on area $a \times b$) that have radii normally distributed around $\langle R \rangle = 0.1\ \mu$m. A pore is in the empty state, E, when there is at most a thin fluid film on the surface. It is in the filled state, F, after capillary condensation. The pores are coupled by the strain on the absorbent that is caused by forces due to the fluid configurations.

Additionally, mesoscopic phenomenologies often allow one to explore parameter domains beyond that of their initial inception and correlate seemingly unrelated observations. The dynamics of a Berea sandstone is a case in point [3].

In preparation for describing the modeling let us look at some of the underlying physical events that take place in porous materials. Consider a porous sample (the adsorbent) having *clean, smooth* surfaces that is under vacuum and held at temperature T. Introduce a small quantity of the gas phase of a material that will *wet* the surface of the sample [8]. The material which is on the surface of the absorbent, typically self-bound as a liquid, is the adsorbate. That the adsorbate wets the surface means that there is an energy advantage for the adsorbate to reside on the adsorbents surface. Consequently, there will be forces of tension in the adsorbent that attempt to expand its surface area. If more gas is admitted into the sample chamber, the adsorbate on the pore wall thickens to become a cylindrical annulus of liquid with one surface held advantageously against the adsorbent and the second surface, the free surface toward the pore center, costing the liquid surface energy [9]. The free surface tries to pull the adsorbate toward the pore center. The adsorbent pulls back. That is, the cylindrical annulus of adsorbate tries to pull the walls of the adsorbent into the pore space. Forces of compression are exerted by the adsorbate on the adsorbent. These forces are in addition to the tensions (parallel to the surfaces) caused by wetting (Fig. 1).

Quite possibly the cylindrical annulus of liquid is energetically more expensive than an alternative liquid configuration, for example, a *capped* cylinder, a pore full of liquid with surface energy costs only at the pore ends [9,10]. Both liquid configurations, cylindrical annulus and capped cylinder, are mesoscopic configurations having energies much greater than $k_B T$, where k_B is the Boltzmann constant. A transition between the two is unlikely to occur due to thermal fluctuations. However, it will occur when the cylindrical annulus becomes absolutely unstable, that is, when there is no restoring force for oscillations of its surface. On making transition to the capped cylinder configuration the liquid comes under tension from the forces associated with the meniscus at the pore ends. These forces, delivered by the liquid to the walls of the adsorbent, try to pull the adsorbent into the pore space.

To here we have sketched the evolution of fluid configurations as more gas is admitted to the sample chamber, the chemical potential of the adsorbate increased from near $-\infty$ to that of saturated vapor, the chemical potential of bulk liquid. [We adopt the convention in which chemical potentials are measured from the chemical potential of bulk liquid at T. Consequently, the chemical potentials will be in the range $-\infty < \mu \leqslant 0$ unless otherwise specified.] If now gas is withdrawn from the sample chamber an equally elaborate sequence of events takes place in which fluid configurations change and in which forces on/in the absorbent change. We do not step through this sequence of events in detail.

The description above is with prejudice. It asks, "How do the fluid configurations change the forces?" In a balanced treatment, one also asks, "How do the forces change the fluid configurations?" In this paper we address both questions.

A coupled fluid-elastic system is driven by two independent fields, the stress σ and the chemical potential μ. The principal response to the stress is the strain, ϵ, and the principal response to the chemical potential is the moisture content, u. We take the system to be in a sequence of states in response to the fields (σ,μ) which are thermodynamic states. By this we mean that when the system is in a state we can, in principle, make *infinitesimal changes* in (σ,μ) that can be recovered on reversal, for example, a low amplitude sound wave in a sandstone that would be described by Biot theory [11]. However, there are changes of state. Both the fluid configurations and the elastic behavior admit the possibility of changes that are not recoverable on reversal. We say these changes are due to *coarse changes* in (σ,μ). In the case of certain materials, for example, a sandstone, the dividing line between infinitesimal and coarse stress perturbations is known [12]. For perturbations of μ there is little guidance from experiment except possibly from work involving superfluids [13]. Nonetheless, we proceed as if the distinction can be respected in modeling and experiment. We will consider (σ,μ) protocols that are coarse in nature. For these there will be irreversible changes in the elastic behavior and in the behavior

TABLE I. Models I, variables. The first row is a list of the variables used in description of a fluid system and in the second row is a similar list for an elastic system. The six columns are (a) the applied field that drives the system, the chemical potential μ and the stress σ; (b) the basic unit of the system that is used in the modeling; (c) the property of the basic unit that is the response to the drive, the moisture content u_i, and the mechanical variables (displacement, strain, and stress) $(x_i,\epsilon_i,\sigma_i)$; (d) the binary variable that specifies the state of a basic unit [for example, $\eta(\tau)=+1 \rightarrow$ closed (full), $\eta(\tau)=-1 \rightarrow$ open (empty)]; (e) the single particle field, generically h_i, to which the state variable responds (the superscript P denotes the possible need for a Preisach bookkeeping space, that is, that a basic unit may respond to different values of the single particle field according to its state); and (f) the rule for the evolution of the state variable that depends on the relationship of the driving field and the single particle field. In the case of a fluid system the basic units respond to the applied field, the chemical potential μ. In the case of an elastic system the basic unit responds to the stress it carries, σ_i. The $\hat{*}$ in columns (e) and (f) are reminders that each basic unit may be sensitive to values of the single particle field that are specific to it, for example, pore geometry, location in the elastic system, microscopic elastic details such as microcracks, etc. The single particle field that enters the rules for change of state may be the single particle field from (e) or an effective single particle field that has a contribution due to coupling (see Table II).

(a) Applied field	(b) Descriptive unit	(c) Local response of unit	(d) State variable of unit	(e) Single particle field	(f) Rule for state change
μ	Pore or element having moisture response	u_i	τ_i	$h_i \leftrightarrow \hat{\mu}_i$, $\hat{\mu}_i^P$	$(\tau_i)\mu \leftrightarrow h_i$, $(\hat{\mu}_i,\hat{\mu}_i^P)$
σ	Elastic element	x_i,ϵ_i,σ_i	η_i	$h_i \leftrightarrow \hat{\sigma}_i$, $\hat{\sigma}_i^P$	$(\eta_i)\sigma_i \leftrightarrow h_i$, $(\hat{\sigma}_i,\hat{\sigma}_i^P)$

of fluid configurations. We assign these changes to elastic elements and to fluid elements. These elements have various manifestations; they may be cylindrical pores, sets of wood cells, or groups of microfibrils.

The irreversible changes in the elastic state of an elastic element and irreversible changes in the fluid configuration of a fluid element are essentially binary, a microcrack is closed or open, a pore is full or empty (has only a surface layer of fluid). Thus, an essential ingredient of the description is an Ising variable $\eta_j = \pm 1$ that specifies the elastic state of each elastic element and an Ising variable $\tau_i = \pm 1$ that specifies the fluid state of each fluid element. The distinction between infinitesimal and coarse from above is between changes in σ (μ) that leave the set of τ (η) unchanged (infinitesimal) or not (coarse). The state of the system is specified by the set of elastic element states and the set of fluid element states. The elastic element states and the fluid element states change according to sets of rules, described below, that relate the effective single particle field the element experiences to a critical value of that field. See Table I and below.

We are particularly concerned with modeling coupled fluid-elastic systems. There are in principle four couplings of interest. These are displayed in Table II. The two diagonal couplings are $J_{ij}\tau_i\tau_j$, the coupling of fluid element i to fluid element j, and K_{ij}, the coupling of displacement x_i to displacement x_j. The two off-diagonal couplings are $u_i R_{ij}\eta_j$ $(x_i P_{ij}\tau_j)$, the coupling of elastic (fluid) element j to fluid (elastic) element i. We examine the consequences of the couplings in a sequence of three cases. These are (1) a model of a coupled fluid-elastic system, using hysterons, that lets us examine important features with a minimum of computational detail (Sec. II); (2) a finite element model of an elastic system into which we introduce internal forces that lead to hysteresis (Sec. III); and (3) a finite element model of a coupled fluid-elastic system again with internal forces (Sec. IV). Models (2) and (3), in contrast to model (1), in which hysteresis is due to hysterons, have hysteresis because of the interactions between elastic (fluid) elements.

II. HYSTERONS

Coupled fluid-elastic system. We describe a porous system in terms of global variables, the strain of the system, ϵ, the moisture content of the system, u, an average stress on the system, σ, and the chemical potential in which the system resides, μ. The system has no spatial structure. [Contrast this with finite element modeling below.] The justification for this

TABLE II. Models II, coupling. The variables used to describe the fluid system are moisture content u and fluid state τ. The variables used to describe the elastic system are the elastic state η, the strain ϵ, and the displacement x. There are four possible couplings. (1) Within the fluid system J_{ij} couples the moisture state of pore i with the moisture state of pore j. (2) Within the elastic system K_{ij} couples the displacement of node i to the displacement of node j, and the internal forces Q_{ij} couple the elastic state of element j to the displacement of node i [see case (2) in the text]. (3) Fluid-elastic coupling. The first entries in the off-diagonal locations are the generic form of the coupling. The second entries are specific examples of the coupling that are described in the text as cases (1) and (3). The RFIM would correspond to a fluid, driven by μ, in which the state variable τ_i responds to the effective single particle field $h_i + \sum_j J_{ij}\tau_j$, where the h_i and J_{ij} are specified in suitable fashion [6].

	τ,u	η,ϵ,x
τ,u	$J_{ij}\tau_i\tau_j$	$u_i R_{ij}\eta_j$ $\hat{\mu}_i = -\frac{2\gamma}{R(\epsilon)}$ Case (1)
η,ϵ,x	$x_i P_{ij}\tau_j$ $\hat{\mu}_i = \hat{\mu}_i^0 - \Lambda(\nabla\cdot\mathbf{u})_i$ Case (3)	$K_{ij}x_i x_j$ $x_j Q_{ij}\eta_j$ Case (2)

is that the moisture content in the system is additive over the moisture content of the fluid elements (pores) and the strain of the system is approximately additive over the strain of the elastic elements. To deal with detail in the description of the response of the system to elaborate driving protocols we stay within mean field theory and look at the behavior of each elastic element and each fluid element.

Moisture content. The pore system consists of N pores, $i = 1, \ldots, N$. Each pore can be in one of 2 states, denoted E (for empty) and F (for full), according to the relationship of the chemical potential μ to the chemical potential pair (μ_F, μ_E) associated with the pore. The chemical potential μ_F is the chemical potential at which a pore makes a transition from empty (cylindrical annulus) to full (capped cylinder); the chemical potential μ_E is the chemical potential at which a pore makes a transition from full (capped cylinder) to empty (cylindrical annulus) (Fig. 1). We assume we have available the information necessary to write

$$u = \frac{1}{N}\sum_{i=1}^{N} u_E(i)\,\frac{1-\tau_i}{2} + \frac{1}{N}\sum_{i=1}^{N} u_F(i)\,\frac{1+\tau_i}{2}, \qquad (1)$$

where u is the moisture content, the sum is over pores, $i = 1, \ldots, N$, $u_E(i)$ is the amount of fluid in pore i in the empty ($\tau_i = -1$) state, and $u_F(i)$ is the amount of fluid in pore i in the full ($\tau_i = +1$) state. There is a rule for the evolution of the state variable for each pore, for example, as follows.

(1) If $\tau_i = -1$ and μ passes to above $\mu_F(i)$, then $\tau_i \to +1$.
(2) If $\tau_i = +1$ and μ passes to below $\mu_E(i)$, then $\tau_i \to -1$.
(3) The chemical potential pair associated with each pore $[\mu_F(i), \mu_E(i)]$ is prescribed from physical arguments given below.
(4) It is quite possible that $u_E(i)$ and $u_F(i)$ vary with μ and σ as, for example, in the use of $R(\epsilon)$ in Eq. (7) and $\nabla \cdot \mathbf{u}$ in Eq. (12).
(5) The system is driven by a chemical potential protocol.

Strain. We make a description of the strain in the same style as that of the moisture content. The strain is the sum of the strain of M elastic elements, $i = 1, \ldots, M$, each of which can be in one of two strain states, denoted o (for open) and c (for closed), according to the relationship of the stress σ to a stress pair (σ_c, σ_o) associated with the elastic element. The stress σ_c is the stress at which an elastic element makes a transition from open to closed (think microcrack, asperity set, or similar mesoscopic elastic feature); the stress σ_o is the stress at which an elastic element makes a transition from closed to open. We assume we have available the information necessary to write

$$\epsilon = \frac{1}{M}\sum_{i=1}^{M} \epsilon_o(i)\,\frac{1-\eta_i}{2} + \frac{1}{M}\sum_{i=1}^{M} \epsilon_c(i)\,\frac{1+\eta_i}{2}, \qquad (2)$$

where ϵ is the strain, the sum is over elastic elements, $i = 1, \ldots, M$, $\epsilon_o(i)$ is the strain of elastic element i in the open ($\eta_i = -1$) state, and $\epsilon_c(i)$ is the strain of elastic element i in the closed ($\eta_i = +1$) state. There is a rule for the evolution of the state variable for each elastic element, for example, as follows.

(1) If $\eta_i = -1$ and σ passes to above $\sigma_c(i)$, then $\eta_i \to +1$.
(2) If $\eta_i = +1$ and σ passes to below $\sigma_o(i)$, then $\eta_i \to -1$.
(3) The stress pair associated with each pore $[\sigma_c(i), \sigma_o(i)]$ is prescribed from physical arguments given below.
(4) It is quite possible that $\epsilon_o(i)$ and $\epsilon_c(i)$ vary with μ and σ [see item (4) below Eq. (1)].
(5) The system is driven by a stress protocol.

We note that each fluid element responds to the field μ and each elastic element responds to the field σ. In thermal equilibrium the chemical potential is invariant at all points in a system; it is a global variable. In mechanical equilibrium the stress is fed through a system in an anecdotal way, depending on details of the arrangement of elastic elements; it is a local variable. Thus, the rules here for the evolution of η with σ are a *mean field* approximation. The description in Eqs. (1) and (2) suggest the use of a Preisach bookkeeping space [14]. The fluid system and elastic system are coupled to one another through the dependence of u_E, u_F, ϵ_o, and ϵ_c on μ and σ, as well as the dependence of the critical pairs (μ_F, μ_E) and (σ_c, σ_o) on μ and σ.

Example with details. To illustrate assembly of the ingredients required to carry through the recipes in Eqs. (1) and (2) we look through a particular problem in some detail. We consider the isotherm of a fluid that is coupled to the strain field the fluid configurations cause. The geometry is that shown in Fig. 1. The fluid elements are a set of vertical, nonintersecting pores of length c, having areal density n_A on area $a \times b$. There is no direct pore-pore coupling, $J_{ij} = 0$. The pore radii, R, are drawn from the probability density

$$p(R) = A\exp[-(R - R_0)^2/w^2], \qquad \int p(R)dR = 1,$$
$$\int p(R)\, R\, dR = \langle R \rangle, \qquad (3)$$

where A is a norming constant, $\langle R \rangle = R_0 = 0.1\ \mu$m, and $w = 0.1\ \mu$m. We treat u according to Eq. (1) in detail but make a simple approximation to handle Eq. (2). To wit, for a wetting fluid, in the E state, there is a thin film of fluid on the surfaces of the cylinders. The fluid in the first few layers of the film has lower energy because of proximity to the surface and causes forces that try to increase the amount of surface. These forces (of tension) are present in all fluid configurations beyond those for the thinnest films. They cause a prestrain. Take the radii that are distributed as in Eq. (3) to be for the material with the prestrain in place. The strains we consider are those beyond the prestrain. For a wetting fluid in the F state there are forces of tension on the ends of the fluid columns due to the pressures $p \sim 2\gamma_{LV}/r$, where γ_{LV} is the surface tension and r is the radius of curvature of the end cap. For an approximately uniform spatial distribution of filled pores these forces, communicated to the interior of the sample where they approximately balance one another, result in net compressive forces on the x-z and y-z surfaces (Fig. 1). We write

$$\mathbf{div} \cdot \mathbf{u} = \epsilon_{xx} + \epsilon_{yy} = (\mathbf{div} \cdot \mathbf{u})_T + (\mathbf{div} \cdot \mathbf{u})_C, \qquad (4)$$

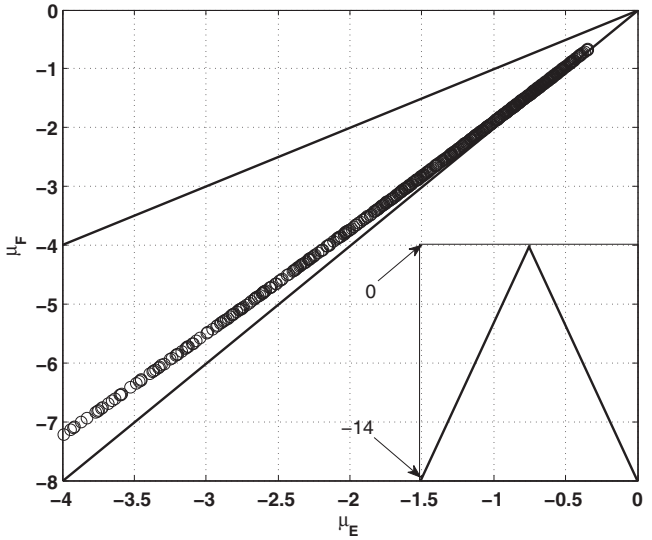

FIG. 2. Preisach space. The chemical potential pairs (μ_F,μ_E) are plotted as open circles. [The values of (μ_F,μ_E) are made dimensionless by scaling by $\gamma_{LV}/(n_L\langle R\rangle)$.] The upper black line is the diagonal $\mu_E = \mu_F$ and the lower black line is at $\mu_E = 2\mu_F$. For a pore of radius R the chemical potential for $F \to E$ is at $-2\gamma_{LV}/(n_L R) \to -2\langle R\rangle/R$. The (μ_F,μ_E) pairs are above the line $\mu_E = 2\mu_F$ because the instability that leads to the $E \to F$ transition is at finite film thickness, that is, at $\mu_F < -\gamma_{LV}/(n_L R) = \mu_E/2$. For pores of large radius $\mu_F \to \mu_E/2$ and $\mu_F \to 0^-$. The inset in the lower right is the μ^* protocol, where the horizontal axis is "time."

with **u** the displacement field, T (C) denoting tension (compression), $(\mathbf{div}\cdot\mathbf{u})_T$ is the prestrain, and

$$(\mathbf{div}\cdot\mathbf{u})_C = -2\sqrt{n_A}\langle R\rangle\frac{\gamma_{LV}}{\kappa\, r}n_F = \Lambda\ |\mu^*|n_F, \qquad (5)$$

where n_F is the fraction of pores in the F state and Λ is a constant having values less than zero. Here κ is the elastic constant of the adsorbent and μ^* is the chemical potential measured in units of $\gamma_{LV}/(n_L\langle R\rangle)$. We get to this result by (1) arguing that the net force on a face of the system is approximately $(\langle R\rangle c)(\gamma_{LV}/r)$ per pore for $a\sqrt{n_A}$ pores and (2) relating the pressure γ_{LV}/r to the chemical potential $|\mu| = \gamma_{LV}/(n_L r)$, where n_L is the particle number density. We modify R according to

$$R \to R[1 + (\mathbf{div}\cdot\mathbf{u})_C] = R(\epsilon) = R(u). \qquad (6)$$

For μ_E we take

$$\mu_E[R(\epsilon)] = -2\frac{\gamma}{n_L R(\epsilon)} \approx -2\frac{\gamma}{n_L R(0)}[1 - (\mathbf{div}\cdot\mathbf{u})_C], \qquad (7)$$

the chemical potential at the $F \to E$ instability of a pore of radius $R(\epsilon)$ [10]. For μ_F we want the chemical potential of the $E \to F$ instability. This instability is associated with the fluctuations of the fluid surface in the empty pore configuration. The values of μ_F scale approximately as $-\gamma_{LV}/R(\epsilon)$ and are found from numerical study [10] (see Fig. 2). Thus, the fluid elements are coupled to the average fluid state of the system [Eqs. (5)–(7)] through the dependence of the (μ_F,μ_E) pairs on the strain.

To complete the description of the system we need the moisture content of an element in the E and F states; $u_E(i) \sim R_i(\epsilon)h_i[R(\epsilon)]$ and $u_F(i) \sim R_i(\epsilon)^2$, where $h(R)$ is the thickness of the fluid film in a pore of radius R in the state E at μ. We begin with all pores in the state $\tau_i = -1$, corresponding to $\mu \to -\infty$ and follow the system through the chemical potential protocol shown in the inset in Fig. 2. [The state of the fluid system is set by the chemical potential, μ. The chemical potential is proportional to $\ln(P_v/P_{sv})$, where P_v is the pressure of the unsaturated vapor in which the sample resides and P_{sv} is the saturated vapor pressure at T. The ratio P_v/P_{sv} is defined to be the relative humidity, R_H. Thus, $\mu \propto \ln(R_H)$ and $\mu = 0$ at $R_H = 1$. A third quantity used to characterize the state of the fluid system, the *capillary pressure*, p, is essentially the chemical potential since, when p can be defined, $n_L p = -\mu$. We use μ in description of the physics and μ and R_H to show results.]

We show the results of carrying the system through the chemical potential protocol in Fig. 3, u as a function of R_H, and Fig. 4, the compressive strain as a function of μ^*. In both figures the results for $\Lambda = 0$ and for $\Lambda = -0.025$ are shown. In the figure of $u - R_H$ the open circle curve for $\Lambda = 0$ shows an adsorption isotherm that is determined by the simple rules for filling and emptying pores that are below Eq. (1) and embodied in the Preisach bookkeeping space in Fig. 2. The state of the pore system is additive over the state of the pores, is hysteretic because the pores are individually hysteretic, exhibits end point memory, and exhibits congruence (not shown). These properties follow from the fact that the Preisach space is static, that is, the pair (μ_F,μ_E) for each pore remains unchanged as the system is taken through the μ protocol. The case $\Lambda = 0$ is trivial in Fig. 4; there is no

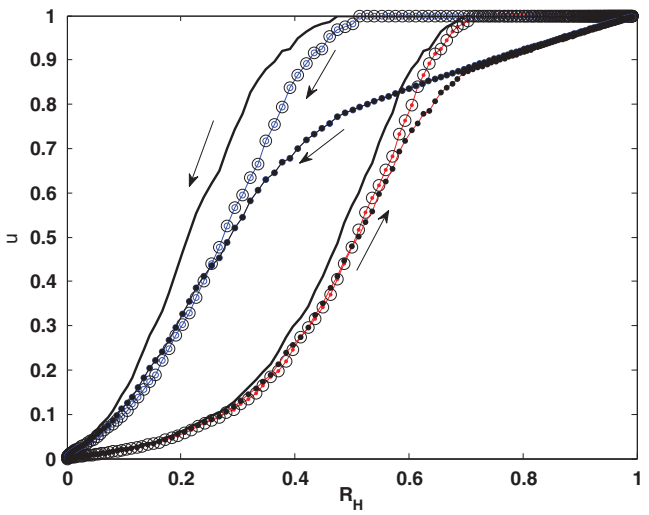

FIG. 3. (Color online) Moisture content as a function of relative humidity. For no interaction between pores, $\Lambda = 0$ in Eq. (5), the isotherm (open circles) is controlled entirely by the (μ_F,μ_E) pairs. For $\Lambda = -0.025$ the interaction distorts the isotherm (solid circles), particularly at $u > 0.8$ where the interaction is very strong. The approximately linear behavior of u near $R_H \to 1$ is due to the change in pressure that occurs when all pores are full of fluid and $r \to +\infty$, where r is the radius of curvature of liquid at the pore end. The curve without symbols is for the case that (μ_F,μ_E) shift with the strain as in Eq. (5) but the pore radii are taken as unchanged in the calculation of u.

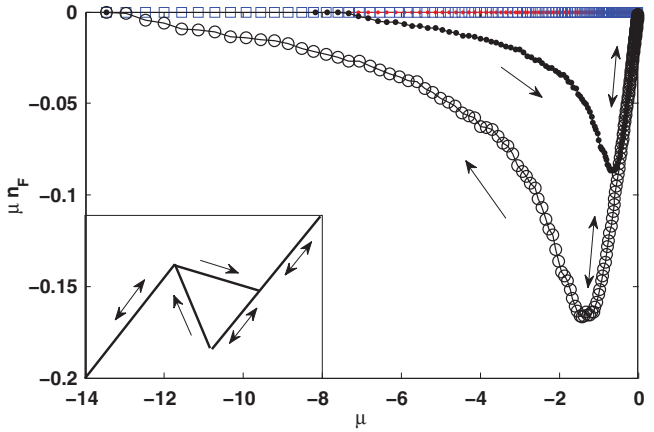

FIG. 4. (Color online) Compressive strain. The moisture dependent term in the compressive strain, Eq. (5), is plotted as a function of μ^* for the two isotherms in Fig. 3, $\Lambda = 0$ (open square at 0) and $\Lambda = -0.025$ (solid circles for μ increase and open circles for μ decrease). The arrows show the direction of the chemical potential change along the curves. There is reversible change in strain with change in chemical potential along the double-tipped arrows, that is, no change in state. As is often the case the *strain stays in*. The inset is a schematic representation of the strain-μ result of Amberg and McIntosh [15,16].

strain [Eq. (5)]. When $\Lambda = -0.025$ the closed circle curve in Fig. 3 is found. This isotherm differs from the $\Lambda = 0$ isotherm noticeably at $u > 0.6$. At $R_H > 0.7$, $n_F = 1$, and u is reversible. The change in u from $0.7 < R_H < 1.0$ is due to the change in the volume of the pore space brought about by the compressive stress (see Fig. 4). Below $R_H \approx 0.6$ the $\Lambda = 0$ and $\Lambda = -0.025$ isotherms are very similar. The behavior of u for $\Lambda < 0$ involves both the compression, leading to less fluid in the pores, and the shift of μ_F to more negative values. This is confirmed with the black curve in Fig. 3; u calculated for the artificial case that the (μ_F, μ_E) pair shifts with the strain as in Eq. (7) but that the pore radius is unchanged in the calculation of u. The strain seen in Fig. 4 is in qualitative accord with the measurements of Amberg and McIntosh [15] and recently [16] (see the inset in Fig. 4).

III. FINITE ELEMENT ELASTIC MODEL

Finite element model of an elastic system. Above we introduced a model of the coupled fluid-elastic system and illustrated an implementation of the model which focused on the fluid. Here we shift to finite element modeling [17] and further shift to look only at the elastic system (see Fig. 5). That system comprises $j = 1, \ldots, M$ constant strain triangular elastic elements [17] that result from a mesh over the area $a \times b$ (compare Figs. 1 and 5). All elastic elements have the same isotropic elastic properties, E (the Young's modulus) and ν (the Poisson ratio). To have the analog of the set of discrete displacements hysterons [18], that are used in the modeling of hysteretic elastic systems, we introduce a set of internal forces. There is one set of forces associated with each elastic element that (a) are on the nodes of the elastic element, (b) are proportional to the distance from element centroid to node, (c) are in the direction from element centroid to node, and

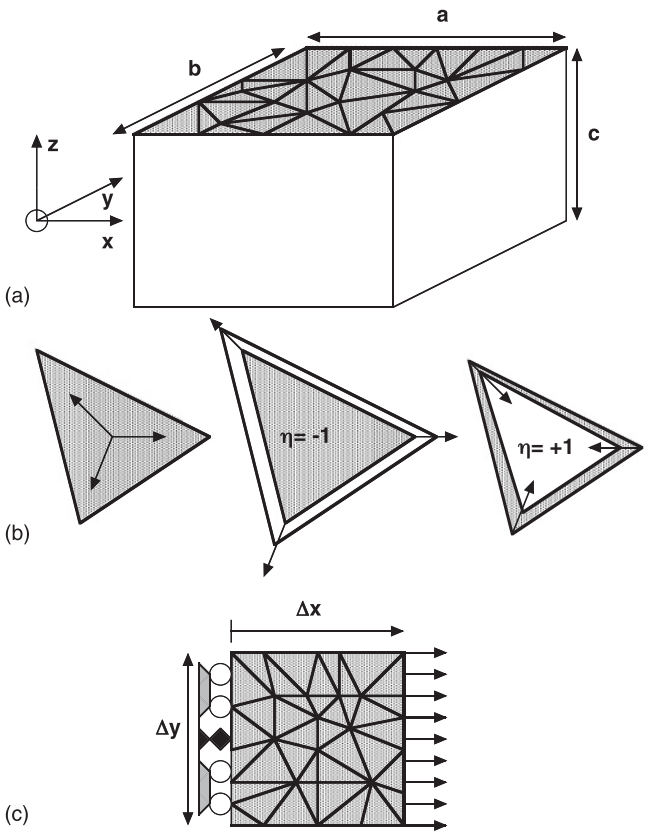

FIG. 5. Elastic system. (a) The triangular elastic elements are elastically identical having elastic constants $(E, \nu) = (1.0, 0.3)$. (b) Each elastic element carries a set of three internal forces that are along the line from triangle centroid to vertex and can at most change sign, $\eta = \pm 1$. (c) The system is tethered at $x = 0$ on the left and in $y = 0.5$ at the left center. It is driven from the right-hand side by a force protocol. The x strain is defined as the change in the average x displacement of the right-hand side. The y strain is defined as the change in the average y separation of the top and bottom.

(d) have sign $\pm$ determined by the state of the elastic element. Thus, there is a state variable associated with each elastic element, $\eta_j = \pm 1$, which controls the sign of the internal forces that an element exerts on its nodes. When the state of an elastic element is $\eta = -1$ the forces on the nodes of the element are outward (tensile) and when the state of an elastic element is $\eta = +1$ the forces on the nodes of the element are inward (compressive) (Fig. 5). The rules for the behavior of the state variable are as follows (where one could read o = open and c = closed).

(1) If an elastic element is in state $\eta_j = +1$ and the stress supported by the elastic element (the internal stress) passes to above $\sigma_o(j)$, $\eta_j \to -1$.

(2) If an elastic element is in state $\eta_j = -1$ and the stress supported by the elastic element (the internal stress) passes to below $\sigma_c(j)$, $\eta_j \to +1$.

Like the modeling above this model suggests the use of a Preisach bookkeeping space. The stress pair for each elastic element (σ_o, σ_c) is determined by a model of the elastic features in the elastic element which confer hysteretic behavior on it. The important difference between the model here and that above is that the field that determines the behavior of an elastic

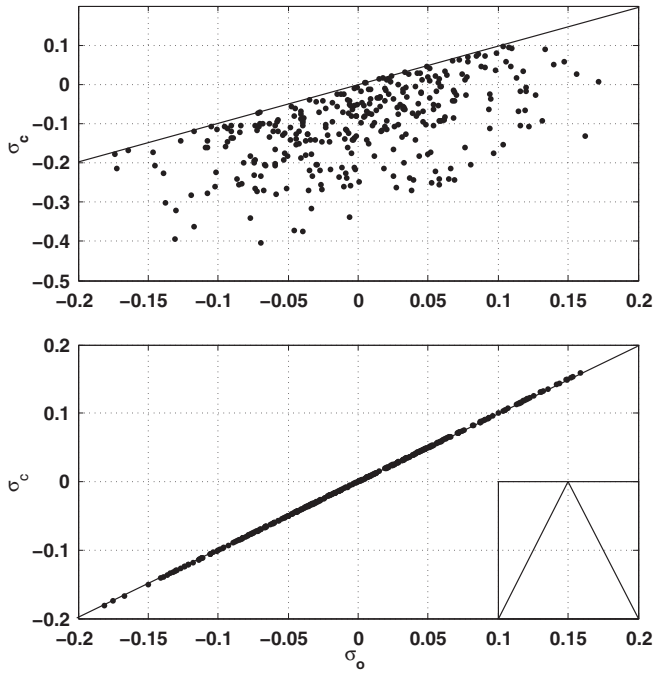

FIG. 6. (σ_o,σ_c) Preisach space. (Top) Preisach space with off-diagonal elements, $\sigma_c \leqslant \sigma_o$, used in the calculations leading to the results in Fig. 8 (left panels). (Bottom) Preisach space with diagonal elements only, $\sigma_c = \sigma_o$, used in the calculations leading to the results in Fig. 8 (middle, right panels). (Inset) Schematic of μ protocol used in all calculations.

element is not the mean field associated with the system, the applied stress, but rather the stress the elastic element supports. A sketch of the finite element equations we employ is given in the Appendix.

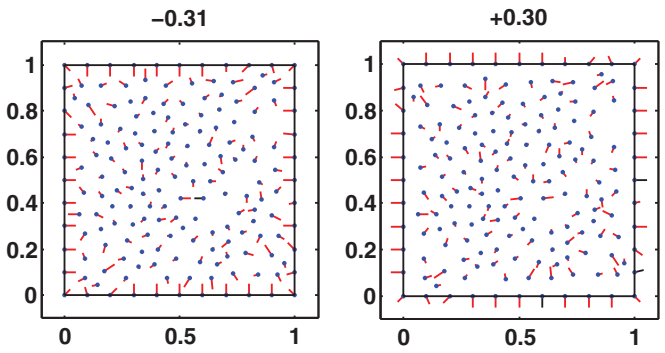

FIG. 7. (Color online) Forces on system. Each node experiences a net internal force which is the sum of the forces from the elements that touch it. (Left) The net internal forces are shown as lines pointing from the nodes (dots) at applied stress $\sigma_{xx} = -0.31$ (a compressive applied stress with most elastic elements in the $\eta = +1$ state). (Right) The net internal forces are shown as lines pointing from the nodes (dots) at applied stress $\sigma_{xx} = +0.30$ (a tensile applied stress with most elastic elements in the $\eta = -1$ state). Note, the internal forces on a node are in random directions and typically balanced (small) in the interior of the system in both cases. The forces are unbalanced primarily on the system surface where they point mostly inward (outward) on the left (right).

Example with details. To illustrate the assembly of the ingredients required to carry through the recipe above we look at a particular problem in some detail. The elastic elements are 328 triangles (involving 185 nodes) of a mesh over a 1×1 space, $M = 328$, $N_n = 185$. (There are $3M/N_n \approx 5$ elastic elements sharing a node.) We work near the fiducial stress $\sigma = 0$ with stress scaled so that the values of the critical stresses (σ_c,σ_o) are small compared to 1. Similarly, we choose the strength of the internal forces so that the stresses they produces are of the same order as the critical stresses; that is, we want to easily see the working of the internal forces. Each elastic element is assigned the Young's modulus E and Poisson's ratio ν, $(E,\nu) = (1,0.3)$. We take σ_o normally distributed around $\sigma_o = 0$ with width $w = 0.070$, that is,

$$P(\sigma_o) = C\exp\bigl(-\sigma_o^2/w^2\bigr), \qquad \int d\sigma_o\ P(\sigma_o) = 1. \quad (8)$$

The probability density $P(\sigma_c)$ is similarly distributed with $\sigma_c \leqslant \sigma_o$ (Fig. 6). The system is driven by the applied stress caused by a uniform set of forces applied to the nodes on its right edge (Fig. 5). The applied stress protocol is shown in the inset in the lower right of Fig. 6. It starts at $\sigma_{xx} < \min(\sigma_o)$. Thus, initially $\eta = +1$ for all elastic elements. We monitor the behavior of the system with the x strain (the departure of the average position of the right edge of the system from its initial value) and the y strain (the *change* in the separation of the average position of the top edge form the average position of the bottom edge). The changes in state of an elastic element are made when σ_{xx} in the element pass (σ_o,σ_c), as described in the rules above.

Preliminary to looking at certain results in some detail we call attention to Fig. 7, where we show the internal forces on each node of the system when it is in compression (tension) due to the applied stress. When in compression (tension) most of the elastic elements are in the $\eta = +1$ ($\eta = -1$) state. The forces an element exerts on itself try to compress (expand) the element. By construction, the sum of the forces that an element exerts on its nodes is zero. Consequently, regardless of the state of the set of elements, the internal forces exert no net force on the system. The internal forces tend to cancel in the interior of the system (each interior node feels the force from the approximately five elastic elements arrayed around it). The internal forces appear primarily as surface forces that try to uniformly compress (expand) the system. [The argument leading to Eq. (5) are supported by Fig. 7.]

We look at the behavior of the x and y strains for three cases in Fig. 8 to bring out the role played by the internal forces.

(1) Take the system through the stress protocol using the *off-diagonal* (σ_c,σ_o) distribution in Fig. 6 (top) and the applied stress version of the change of state rules, that is, the applied stress is used in place of the internal stress in the rules. See the $\epsilon - \sigma$ curves in Fig. 8 (left panels).

(2) Take the system through the stress protocol using the *diagonal* (σ_c,σ_o) distribution in Fig. 6 (bottom) and the applied stress version of the change of state rules; that is, the applied stress is used in place of the internal stress in the rules. See the $\epsilon - \sigma$ curves in Fig. 8 (center panels).

(3) Take the system through the stress protocol using the *diagonal*(σ_c,σ_o) distribution in Fig. 6 (bottom) and the internal stress version of the change of state rules, that is, the rules in

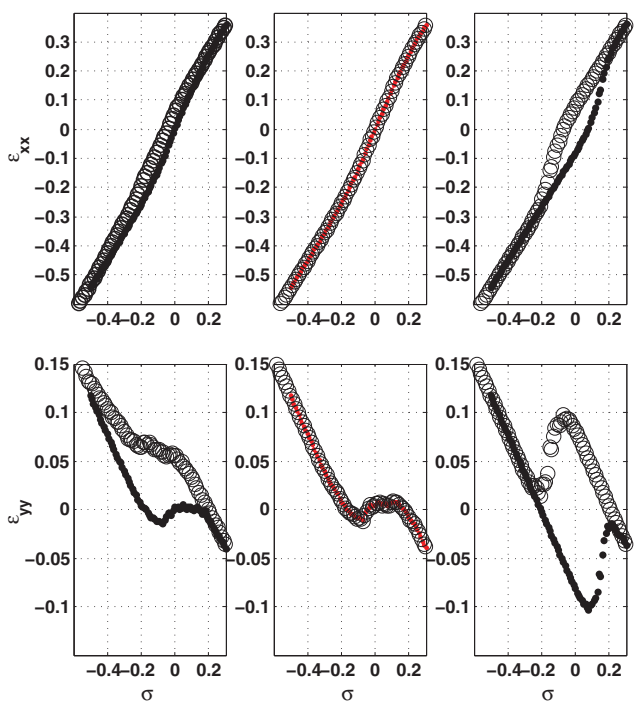

FIG. 8. (Color online) Strain vs applied stress. For all panel sets (top) is the x strain as a function of stress and (bottom) is the y strain as a function of stress. (Left two panels) The strength of the internal forces is nonzero and the Preisach space is *off-diagonal*. (Center two panels) The strength of the internal forces is zero and the Preisach space is *diagonal*. (Right two panels) The strength of the internal forces is nonzero and Preisach space is *diagonal*. The stress protocol in all cases is that shown in the inset in Fig. 6 (bottom) and in all cases $\Lambda = 0.035$.

the first paragraph of this section. See the $\epsilon - \sigma$ curves in Fig. 8 (right panels).

When there are no internal forces that can expand/contract the elastic elements, we have $\epsilon_{xx} \propto \sigma_{xx}$ and $\epsilon_{yy} \propto -\sigma_{xx}$. In the presence of internal forces, as the stress crosses over values of (σ_o,σ_c) that deploy them, the stress-strain relation steps from one $\epsilon \propto \sigma$ curve to a second $\epsilon \propto \sigma$ curve. In the case of the stress protocol being used here the system begins at negative stress with internal forces that try to hold it in a compressed state. While in this state the elastic elements respond with $\epsilon \propto \sigma$. Near $\sigma = 0$ the internal forces switch from compressive to tensile and bring about additional displacements and a transition from one $\epsilon \propto \sigma$ curve to another. Once the internal forces are primarily tensile (they try to hold the system in the tensile state) further response to stress is $\epsilon \propto \sigma$ with the same slope as in the compressed state. For case (1), the switch from compressed state to tensile state occurs as the *applied stress* crosses over the range of values of σ_o. The switch from tensile state to compressed state, on the second leg of the stress protocol, occurs as the *applied stress* crosses over the range of values of σ_c. The strain curves are hysteretic because for any elastic element $\sigma_c \leqslant \sigma_o$ (see Fig. 8). The hysteretic response of the system to stress arises from the hysteretic response of the individual elastic elements to the applied stress. These observations are confirmed with the result for case (2) [Fig. 8 (center)], for which the elastic elements respond to the *applied stress* but $\sigma_c = \sigma_o$; there is no hysteresis in the response of the elastic elements. The working of the internal forces is seen as a reversible displacement near $\sigma \approx 0$ that carries the system from one $\epsilon \propto \sigma$ curve to another.

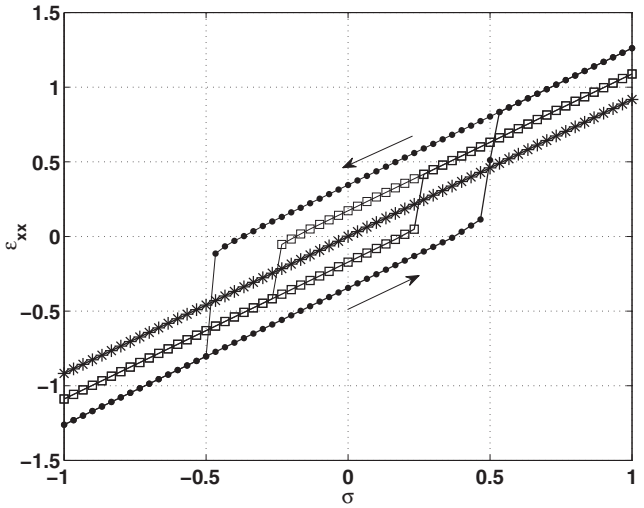

FIG. 9. Effect of internal forces. The x strain as a function of stress for three values of the internal force, $\Lambda = 0$ (asterisks), $\Lambda = 0.1$ (open squares), and $\Lambda = 0.2$ (solid circles). The Preisach space is diagonal. The elastic elements respond to the *internal* stress. The hysteresis loops are sharp because of the strength of the internal forces (compare to Fig. 8). If this circumstance obtained in physical realizations the sharp step, a mechanical avalanche, would be associated with a burst of acoustic emission.

With this preparation we look at case (3); the Preisach space is diagonal and the change of state of the elastic elements involves the *internal stresses* [see Fig. 8 (right)]. The stress-strain curve is hysteretic, its hysteresis being conferred by interaction among elastic elements. The explanation for this behavior is that the internal forces act as a local stress field that adds to the applied stress to produce an effective stress which will change the elastic state at σ_o. When the system starts with all elastic elements in state $\eta = +1$ and the applied stress is brought up from below the local stress works to oppose the changes in applied stress. The change in state from $\eta = +1$ to $\eta = -1$ is at

$$\sigma = \sigma_{\text{applied}} + \sigma_{\text{internal}} > \sigma_o, \tag{9}$$

$$\sigma_{\text{applied}} > \sigma_o - \sigma_{\text{internal}} = \sigma_o + \eta|\sigma_{\text{internal}}| > \sigma_o, \tag{10}$$

where the sign on the right-hand side is chosen knowing that for $\eta = +1$ the internal stress is negative (e.g., Fig. 7). Thus, an elastic element that might change elastic state at $\sigma_{\text{applied}} = \sigma_o$ is trapped in its present state by a stress field that the present state supports. We term this behavior *self-trapping*. It is the source of the hysteresis in Fig. 9. (An analogous argument applies to the response of the elastic elements to stress as the applied stress is brought down from above.) In Eq. (10) we have an effective σ_o that depends on σ in a way which produces much the same effect as an off-diagonal Preisach space. Because of this dependence we should expect the details of the strain as a function of stress to depend on the strength of the internal forces. Indeed, this is the case as seen in Fig. 9. As a final illustration of the behavior of the of the model in case (3) we

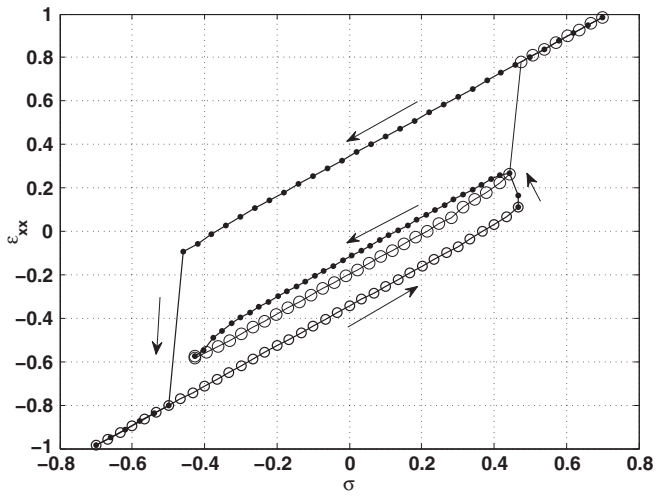

FIG. 10. End point memory. The x strain as a function of stress. For this case the interaction was taken to be very strong so that the transition of the internal forces from closed (compressed) to open (in tension) is very abrupt (compare to Figs. 8 and 9).

show evidence of *end-point memory* in Fig. 10. The model we are dealing with is qualitatively similar to the random field Ising model (RFIM) [6] at $T = 0$.

IV. FINITE ELEMENT FLUID MODEL

Finite element model of coupled elastic-fluid systems. Let us adapt the finite element model above to the case of a coupled elastic-fluid system. We do this having in mind systems typified by wood, in which (for low moisture content) the fluid configurations are not pools of liquid but rather H_2O molecules in cellulose fibrils, cell walls, tracheids, etc. [4]. Thus, the fluid elements are contiguous with the elastic elements. We use *element* in place of either elastic element or fluid element. The system comprises $j = 1, \ldots, M$ triangular elements that result from a mesh over the area $a \times b$ (compare Figs. 1 and 5).

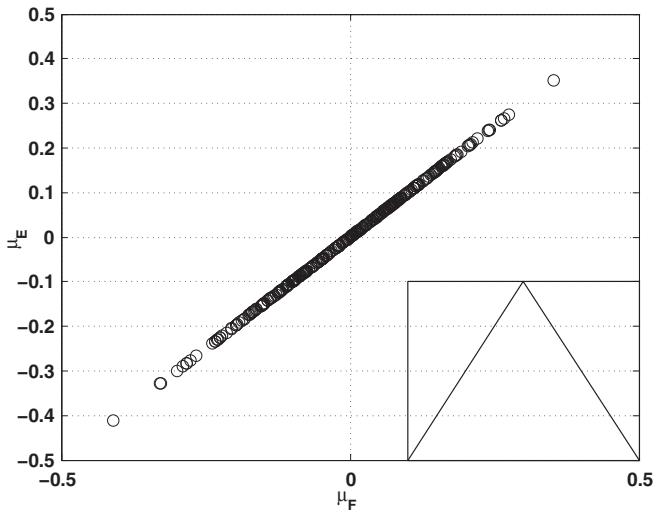

FIG. 11. (μ_F, μ_E) Preisach space. The pairs $(\mu_F, \mu_E = \mu_F)$ used for the studies in Figs. 12 to 17. (Inset) Schematic of the μ protocol used in Figs. 12 to 16.

All elements have the same isotropic elastic properties, K (the Young's modulus) and ν (the Poisson's ratio). All elements have a moisture content that is a function of their geometry. There is a set of internal forces associated with each element that (a) are on the nodes of the element, (b) are proportional to the distance from element centroid to node, (c) are in the direction from element centroid to node, and (d) have sign $\pm$ determined by the state of the element. Thus, there is a state variable associated with each element, $\eta_j = \pm 1$, which controls the sign of the internal forces an element exerts on its nodes. When the state of an element is $\eta = -1$ the forces on the nodes of the element are outward (tensile) and when the state of an element is $\eta = +1$ the forces on the nodes of the element are inward (compressive) (Fig. 5). In contrast to the model above of an elastic system, here the rules for the behavior of the state variable are *driven by the chemical potential*. We begin with rules appropriate to a wood fiber.

(1) If an element is in state $\eta_j = +1$ and the chemical potential passes to above $\mu_F(j)$, $\eta_j \to -1$,

(2) If an element is in state $\eta_j = -1$ and the chemical potential passes to below $\mu_E(j)$, $\eta_j \to +1$.

The chemical potential pair for each element (μ_F, μ_E) is determined by a model of the chemistry of the adsorbate and of the coupling of that chemistry to the elastic state of the element. We adopt a simple phenomenology

$$\mu_F(j) \to \mu_F(j)^0 - \Lambda(\nabla \cdot \mathbf{u})_j,$$
$$\mu_E(j) \to \mu_E(j)^0 - \Lambda(\nabla \cdot \mathbf{u})_j, \tag{11}$$

where $(\nabla \cdot \mathbf{u})_j$ is the strain on element j. When an element is in state $\eta_j = +1$ it can accommodate no adsorbate; when in state $\eta_j = -1$ it can accommodate an amount of adsorbate given by

$$u_j = \frac{1 - \eta_j}{2} \frac{A_j}{A} (\nabla \cdot \mathbf{u})_j, \tag{12}$$

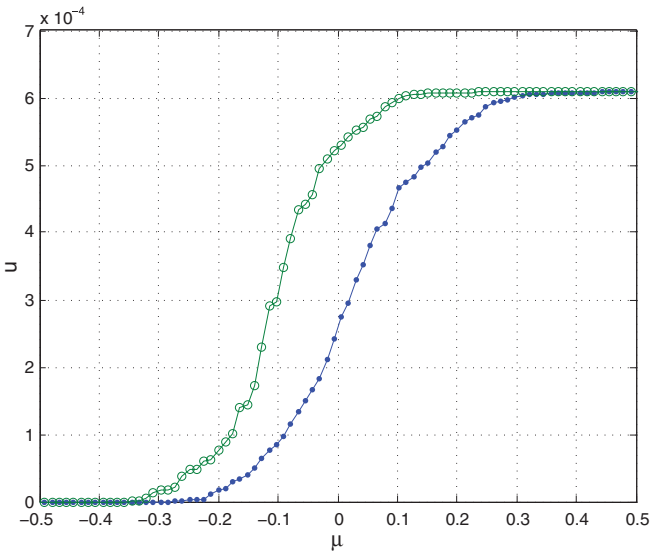

FIG. 12. (Color online) Moisture content vs chemical potential. The moisture content, u, as a function μ for the chemical potential protocol in the inset of Fig. 11 [μ increase (solid circles) and μ decrease (open circles)]. Compare to the strain for the same μ protocol in Fig. 13. The moisture content *stays in*.

where A_j is the area of element j, A is the sum of the areas of the elements, $A = a \times b = 1$, and the first factor accounts for the dependence of u_j on state. The combination of Eqs. (11) and (12) implies that when the chemical potential is such that an element can accommodate adsorbate, make the transition $\eta = +1$ to $\eta = -1$, tensile forces appear locally in the system. These forces contribute to $(\nabla \cdot \mathbf{u})$ throughout the system, making the transition $\eta = +1$ to $\eta = -1$ elsewhere more likely. The feedback between $(\nabla \cdot \mathbf{u})_j$ and $(\nabla \cdot \mathbf{u})$ is a ferromagnetic-like coupling.

Example with details. To illustrate the assembly of the ingredients required to carry through the recipe above we look at a particular problem in some detail. The elements are 328 triangles having 185 nodes, etc., as above. We work near the fiducial chemical potential $\mu = 0$ with chemical potential scaled so that the values of the critical chemical potentials (μ_F, μ_E) are small compared to 1. Similarly, we choose the strength of the internal forces so that the strains they produce make a noticeable change in (μ_F, μ_E). Each element is assigned the Young's modulus E and Poisson ratio ν, $(E, \nu) = (1, 0.3)$. We take μ_F normally distributed around $\mu_F = 0$ with width $w = 0.125$, that is,

$$P(\mu_F) = C\exp\left(-\mu_F^2/w^2\right), \qquad \int d\mu_F \; P(\mu_F) = 1. \quad (13)$$

Like case (2) for the elastic system we introduce no *a priori* hysteresis by taking $\mu_E = \mu_F$. The system is driven by a chemical potential protocol, shown in the inset in the lower right of Fig. 11. It starts at $\mu < \min(\mu_F)$. Thus, initially $\eta = +1$ for all elements. We monitor the behavior of the system with the x strain (the departure of the average position of the right edge of the system from its initial value), the y strain (the change in the separation of the average position of the top edge form the average position of the bottom edge), and the moisture content,

$$u = \sum_{j=1}^{M} u_j. \quad (14)$$

The changes in state of an element are made when the chemical potential passes (μ_F, μ_E) as described in the rules above. [When we put an external force on the system it will be applied, as for the elastic model, uniformly to the nodes on the right-hand side.]

Let us look through a sequence of results. In Figs. 12 and 13 we show u and ϵ_{xx} as a function of μ for the protocol in the inset of Fig. 11. Both u and ϵ_{xx} are hysteretic functions of μ (compare to Fig. 8). The hysteresis, of the *strain stays in* variety, results from the *ferromagnetic-like* interaction of the moisture content with itself. [The rule of thumb *strain stays in* captures the essentials of a hysteretic σ-ϵ curve. As the stress leaves a largest value there is more strain than there was on stress approach to that value. The strain stays in the system.] The system is driven by the chemical potential protocol and the strains observed result from the forces the fluid configurations bring to bear. Because we have made the choice for u_j in Eq. (12), u and ϵ_{xx} behave very similarly as a function of μ, however, not identically. In Fig. 14 u is seen to be a weakly hysteretic function of ϵ_{xx}.

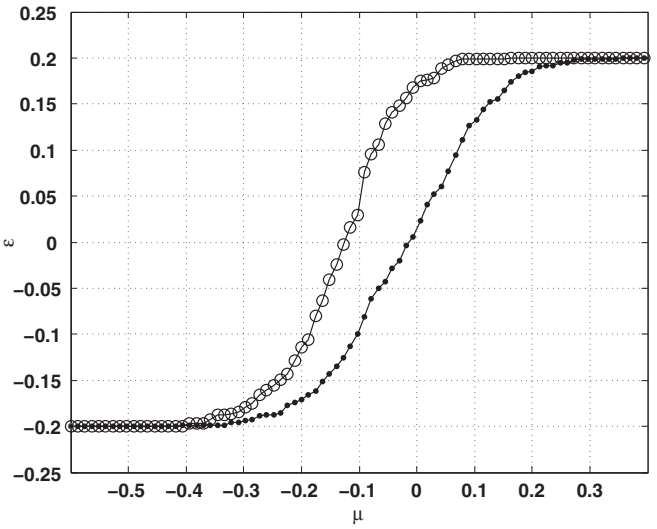

FIG. 13. Strain vs chemical potential. The x strain as a function μ for the chemical potential protocol in the inset of Fig. 11 [μ increase (solid circles) and μ decrease (open circles)]. Compare to the moisture content for the same μ protocol in Fig. 12.

We look a little more closely at the behavior of the system in Fig. 15 where we show the results of a test of congruence for u as a function of μ. A description of the chemical potential protocol used is in the caption to Fig. 15. The two u-μ loops are not equivalent with the lower loop being *fatter*. The secondary response, ϵ_{xx}, exhibits qualitatively similar lack of congruence (not shown).

When the system is strained with an applied stress we expect the capacity for moisture uptake to change. In Fig. 16 we show u as a function of μ for three values of applied force corresponding to $\sigma_{xx} = -0.0025,\ 0.0,\ +0.0025$. All curves were normed to the maximum moisture content at $\sigma_{xx} = 0$. When the system is under compression (solid circles), the

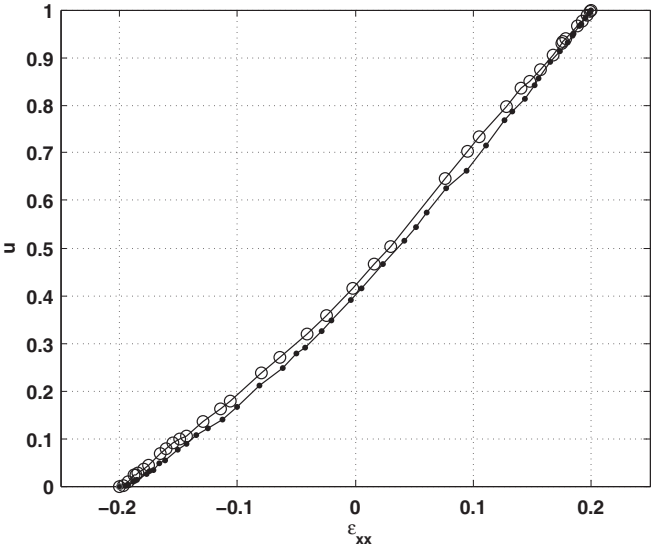

FIG. 14. u-ϵ hysteresis. The moisture content as a function of the strain for the chemical potential protocol in the inset of Fig. 11, μ increase (solid circles) and μ decrease (open circles). See Figs. 12 and 13.

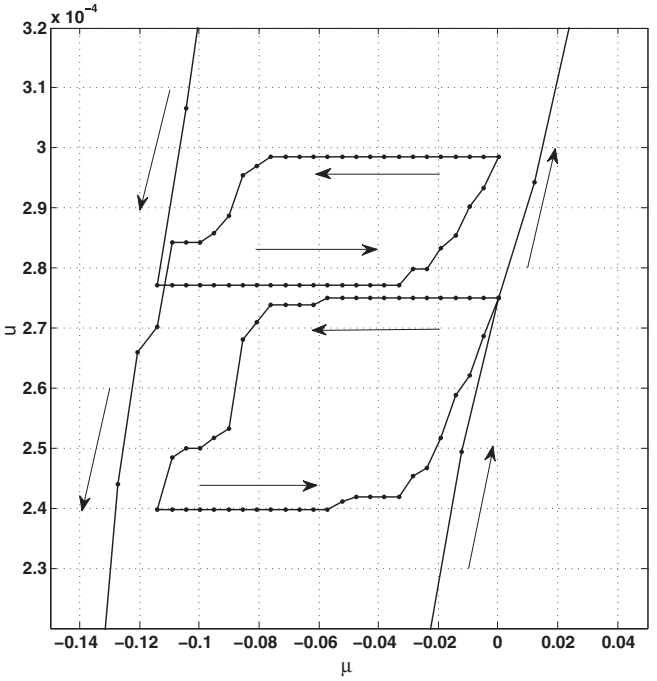

FIG. 15. Congruence test. The moisture content as a function of μ for a modification of the chemical potential protocol in the inset of Fig. 11 to test for congruence. The modification involves two interior loops, $\mu = 0 \rightarrow -0.12^{+} \rightarrow 0$ on μ increase and $\mu = -0.12^{+} \rightarrow 0 \rightarrow -0.12^{+}$ on μ decrease. The part of the u-μ curve not shown overlays that in Fig. 12. There is qualitatively similar lack of congruence in the corresponding strain-μ curve.

volume of the space is reduced and the maximum moisture content is reduced. Just the opposite occurs when the system is under tension (asterisks).

To here we have seen the response of the system to separate chemical potential and applied stress protocols. In Fig. 17 we show the behavior of ϵ_{xx} and u as a function of μ when the system is carried through the mixed (μ,σ_{xx}) protocol shown in Fig. 18. In that protocol the system is brought to $\mu = 0$ under compression, $\sigma_{xx} = -0.0025$, and then carried away and returned to this point around a closed loop in (μ,σ_{xx}). On return to $(0, -0.0025)$ both ϵ_{xx} and u continue on the trajectory that initially brought them to $(0, -0.0025)$. Both ϵ_{xx} and u have end point memory for closed loops in (μ,σ_{xx}) space.

V. CONCLUSION

In this paper we have examined a sequence of models of systems with hysteretic elasticity, hysteretic moisture content, and coupled elasticity and moisture content. It is traditional to get macroscopic hysteresis from the working of an assembly of microscopic hysteretic elements [18]. However, as is known in a different context [6], suspected in the current context [19], and as the models we have introduced show, there is another route to hysteresis. There are circumstances in which systems evolve among mesoscopic structures that are not easily reached from one another. To these the idea of getting macroscopic hysteresis from mesoscopic hysteresis is usefully applied. This is the hysteron limit. There are other circumstances in which

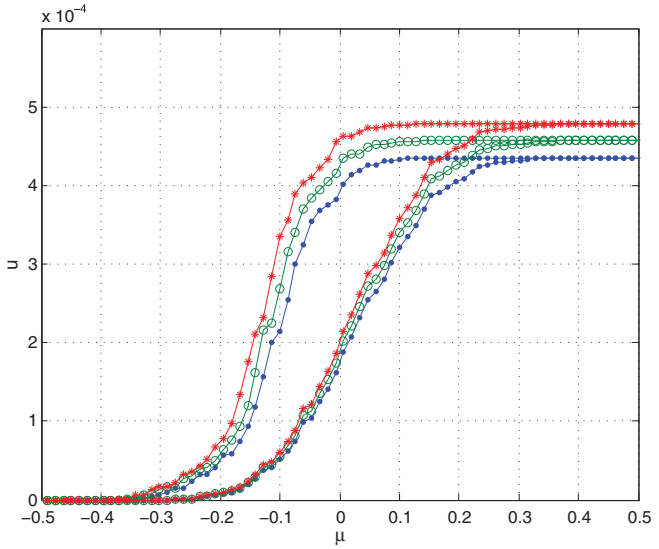

FIG. 16. (Color online) Applied stress. The moisture content as a function of μ for three repetitions of the chemical potential protocol in the inset of Fig. 11 at successively larger applied stress, $\sigma_{xx} = -0.0025, 0.0, +0.0025$ (solid circles, open circles, and asterisks, respectively).

the hysteresis results from the self-trapping of an internal field. This has been illustrated for the elastic model and the fluid model in this paper. The essentials of what is happening are that the critical field values that trigger a change in state, for example, σ_o for the elastic model and μ_F for the fluid model, are modified by the internal forces to maintain the current state. In both limits we consider the coupling between the variables which describe the fluid response and the variables that describe the mechanical response. In the hysteron limit this coupling brings about a quantitative change in features already present without the coupling. In the self-trapping limit it is the coupling that gives rise to the interaction that causes the hysteretic response.

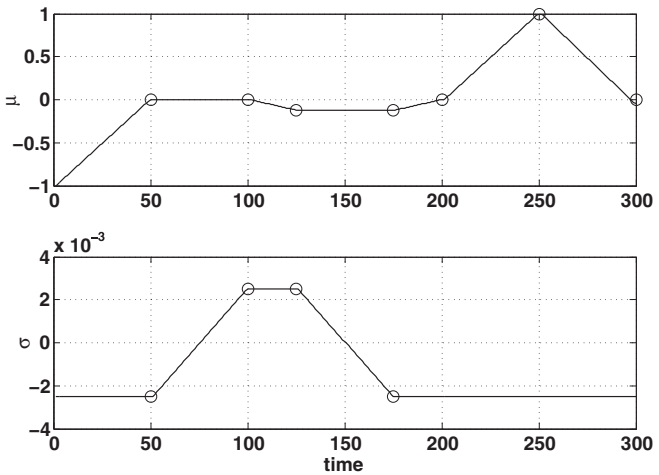

FIG. 17. End point memory (σ,μ) protocol. (Top) The chemical potential as a function of time. (Bottom) The applied stress as a function of time. The chemical potential-stress protocol from $t = 50$ to $t = 200$ is a closed loop in (μ,σ) space. The strain response and moisture response to this protocol are shown in Fig. 17.

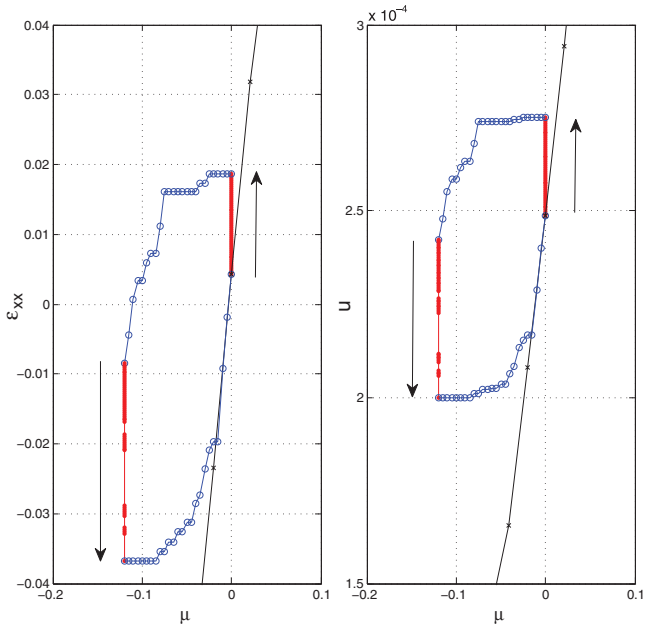

FIG. 18. (Color online) End point memory. The x strain (left) and moisture content (right) as a function of μ for the (μ,σ) protocol in Fig. 18. A closed loop in (μ,σ_{xx}) begins at the feathers of the right arrow (the end of the arrow opposite the tip) and returns to these feathers (50 → 200 in Fig. 18).

In the self-trapping limit a finite element description, which spans three scales, is used. We seek answers on the largest scale (the macroscopic scale 1×1) from calculation at the mesoscopic scale (the scale of an element) that employ forces developed from a picture of the microscopic scale. As no specific scale is introduced this approach can be adapted to the scale of interest. A hierarchical system like wood is a case in point. The mesoscale could be a wood fiber with the microscale corresponding to chemistry within cellulose fibrils. The mesoscale could be that of a wood cell with the microscale corresponding to wood fibers.

APPENDIX

In this appendix we sketch the derivation of a set of finite element equations with emphasis on the construction of the internal forces. For illustrative purposes the system is on a $D = 1$ line $0 \leqslant x \leqslant L$. The equation of motion for the scalar displacement field $u(x)$ is

$$\rho\ddot{u} = \frac{\partial}{\partial x}(K\epsilon) + p(x), \tag{A1}$$

where $p(x)$ are the internal forces (to be specified below) and u is subject to the boundary conditions

$$(K\epsilon)_0 = F, \qquad (K\epsilon)_L = F, \tag{A2}$$

F is the applied force, and $\epsilon = \partial u/\partial x$. The weak form [17] of Eq. (A1) is

$$\int_0^L \delta u\ \rho\ddot{u}\ dx = \int_0^L \delta u\ \frac{\partial}{\partial x}(K\epsilon)\ dx + \int_0^L \delta u\ p(x)\ dx, \tag{A3}$$

which when the first term on the right-hand side is integrated by parts reduces to

$$\int_0^L \delta u\ \rho\ddot{u}\ dx = -\int_0^L \delta\epsilon\ (K\epsilon)\ dx + \int_0^L \delta u\ p(x)\ dx + F(\delta u)_L - F(\delta u)_0. \tag{A4}$$

The finite element equations follow upon representing $u(x)$ in terms of interpolation functions, $H_n(x)$, which connect it to the displacement amplitudes u_n at the nodes $n = 1, \ldots, N$. We write

$$u(x) = \sum_n H_n(x)\ u_n, \quad \delta u(x) = \sum_n H_n(x)\ \delta u_n, \quad \delta\epsilon(x) = \sum_n B_n(x)\delta u_n, \tag{A5}$$

where $B_n(x) = \partial H_n(x)/\partial x$. Use of these equations in Eq. (A4) results in

$$\begin{aligned}\sum_n\sum_m \delta u_n\ddot{u}_m \int_0^L H_n(x)\ \rho H_m(x)\ dx &= -\sum_n\sum_m \delta u_n u_m \int_0^L B_n(x) K B_m(x)\ dx \\ &+ \sum_n \delta u_n \int_0^L H_n(x)\ p(x)\ dx \\ &+ F\sum_n \delta u_n H_n(L) - F\sum_n \delta u_n H_n(0).\end{aligned} \tag{A6}$$

In mechanical equilibrium the term on the left-hand side is zero. The equation for u_s is found by putting all $\delta u_n = 0$ except δu_s, to wit,

$$\sum_m \mathcal{K}_{sm} u_m = F H_s(L) - F H_s(0) + \int_0^L H_s(x)\ p(x)\ dx, \tag{A7}$$

where

$$\mathcal{K}_{sm} = \int_0^L B_s(x) K B_m(x)\ dx \tag{A8}$$

is the stiffness matrix.

For the internal forces, p, we take a sum over p_i a set of force dipoles [20]. The dipole p_i,

$$p_i = f_i\eta_i[\delta(x - b_i + \Delta_i) - \delta(x - b_i - \Delta_i)], \tag{A9}$$

is centered at b_i, has strength f_i, has size $2\Delta_i$, and has a sign that depends on its state $\eta_i = \pm 1$. We take b_i to be at the center of element i and Δ_i such that $b_i \pm \Delta_i$ are the nodes of element i. We identify the state of a dipole with the state of the element it resides on. Then equal and opposite forces will be exerted by p_i on the nodes i and $i + 1$ associated with element i. We have

$$\int_0^L H_s(x)\sum_i p_i(x)\ dx = (2\Delta f)_s\eta_s - (2\Delta f)_{s-1}\eta_{s-1}. \tag{A10}$$

Inserting this equation into Eq. (A7) we have

$$\sum_m \mathcal{K}_{sm} u_m = FH_s(L) - FH_s(0) + (2\Delta f)_s \eta_s - (2\Delta f)_{s-1}\eta_{s-1}. \quad \text{(A11)}$$

This mechanical problem is completed with the rules that relate the state of an element to a property of the element, for example, the stress carried by the element or the moisture state of the element

[1] J. M. Valles, R. H. Higley, R. B. Johnson, and R. B. Hallock, Phys. Rev. Lett. **60**, 428 (1988); Nuclepore is a trademark of Whatman International Ltd.

[2] M. P. Lilly and R. B. Hallock, J. Low Temp. Phys. **101**, 385 (1995).

[3] R. A. Guyer, J. TenCate, and P. Johnson, Phys. Rev. Lett. **82**, 3280 (1999).

[4] J. M. Dinwoodie, *Timber: Its Nature and Behaviour*, 2nd ed. (Van Nostrand Reinhold, London, 2000).

[5] [http://en.wikipedia.org/wiki/Preisach_model_of_hysteresis].

[6] J. P. Sethna, K. Dahmen, S. Kartha, J. A. Krumhansl, B. W. Roberts, and J. D. Shore, Phys. Rev. Lett. **70**, 3347 (1993).

[7] J. C. Toledano and P. Toledano, *The Landau Theory of Phase Transitions*, World Scientific Lecture Notes in Physics, Vol. 3 (World Scientific, Singapore, 1987).

[8] P. G. de Gennes, Rev. Mod. Phys. **57**, 827 (1985).

[9] G. Bertotti and I. Mayergoyz, *The Science of Hysteresis* (Academic Press, Oxford, 2006).

[10] S. M. Cohen, R. A. Guyer, and J. Machta, Phys. Rev. B **33**, 4664 (1986).

[11] D. L. Johnson, Appl. Phys. Lett. **37**, 1065 (1980).

[12] J. A. TenCate, D. Pasqualini, S. Habib, K. Heitmann, D. Higdon, and P. Johnson, Phys. Rev. Lett. **93**, 065501 (2004).

[13] S. M. Cohen, R. A. Guyer, and J. Machta, Phys. Rev. B **34**, 6522 (1986).

[14] F. Preisach, Z. Phys. **94**, 277 (1935).

[15] C. H. Amberg and R. McIntosh, Can. J. Chem. **30**, 1012 (1952).

[16] J. Prass, D. Muter, P. Fratzl, and P. Oskar, Appl. Phys. Lett. **95**, 083121 (2009).

[17] O. C. Zienkiewicz, R. L. Taylor, and J. Z. Zhu, *The Finite Element Method Set*, 6th ed., (Elsevier, Oxford, 2005).

[18] K. R. McCall and R. A.Guyer, J. Geophys. Res. **99**, 23887 (1994).

[19] A. Grosman and C. Ortega, Langmuir **25**, 8083 (2009).

[20] K. Aki and P. G. Richards, *Quantitative Seismology* (University Science Books, Sausalito, CA, 2002).